Nanoscale

RSC Publishing

PAPER

View Article Online
View Journal | View Issue

Cite this: *Nanoscale*, 2013, **5**, 11227

Fabrication of hollow metal oxide nanocrystals by etching cuprous oxide with metal(II) ions: approach to the essential driving force†

Jong Hwa Sohn, Hyun Gil Cha, Chang Woo Kim, Do Kyoung Kim and Young Soo Kang*

Hollow metal oxide nanocrystals were prepared by etching cuprous oxide with metal ions and were applied as photoelectrodes. As a hard template, polyvinylpyrrolidone stabilized cuprous oxide (PVP–Cu_2O) and non-stabilized cuprous oxide (nPVP–Cu_2O) were synthesized by a precipitation method. Hollow iron oxide and cobalt oxide nanocrystals with a truncated octahedral morphology were fabricated by an etching reaction with transition metal(II) ions (Fe^{2+} or Co^{2+}). In the etching reaction process, a cationic exchange reaction occurs between the divalent metal ion and Cu^+ due to the higher Lewis acidity. Facet selective etching of cuprous oxide has been observed during the ionic exchange reaction of Cu^+ and O^{2-} ions in PVP–Cu_2O complexes with transition metal(II) ions (Fe^{2+} or Co^{2+}) at the surface of a (110) facet. Amorphous states of hollow metal oxide products were annealed to form α-Fe_2O_3 (hematite) and Co_3O_4 and their crystal structure was examined with X-ray diffraction and HR-TEM. The optical absorption behavior of semiconductor nanocrystals was measured with UV-vis spectroscopy to define band gap energy. The hollow hematite structure has a 2.08 eV band gap and Co_3O_4 (Co(II,III) oxide) has a 1.80 eV indirect band gap. Using these hollow nanocrystals, a metal oxide monolayer film was fabricated with a secondary growth approach and was studied for its photocatalytic properties.

Received 15th July 2013
Accepted 19th August 2013

DOI: 10.1039/c3nr03626j

www.rsc.org/nanoscale

Introduction

The design and manipulation of the morphology of metals and metal oxides have become an attractive issue and have led to a novel breakthrough in materials chemistry because of their catalytic activity and physiochemical reactivity from a low coordination number of surface atoms at their edge and corner.[1] Dimensionally controlled structures including spheres, cubes, wires, rods, plates and tubes produced by hydro- and solvo-thermal syntheses, chemical bath deposition and electrodeposition have shown unique performance towards photoelectric, magnetic and catalytic properties.[2] Especially, hollow-structured materials have attracted much attention because of their structural features, such as voids, and are promising as for gas sensing,[3] Li-ion batteries,[4] photocatalysts,[5] and dye sensitized solar cell (DSSC) applications.[6] Because of the voids in the hollow structures, they are suitable for controlling the incorporation and release of inorganic and organic moleclues.[7] Moreover, the easy modulation of refractive index, and a lower density and increased active area for catalysis would be also expected from the presence of voids.[8] Up to now, the development of hollow structures has been achieved by using methods based on the Kirkendall effect, template mediated growth or acidic etching processes in various metal chalcogenide or metal alloy materials such as Co_3O_4,[9] Cu_7S_4,[10] Fe_2O_3,[11] Cu_2O,[12] PtPd[13] and PtCu.[14]

Cuprous oxide, Cu_2O, is a promising photo-electric and catalytic material for water splitting, sensors and photocatalytic reactions as a p-type semiconductor with a 2.17 eV indirect band gap energy. Tremendous efforts have been dedicated to the synthesis of cuprous oxides with cubic, octahedral,[15] polyhedral,[16] rod and tube[17] shapes because of their tunable morpho-synthetic properties under relatively mild reaction conditions. The hydrothermal, seed-mediated, electrodeposition and precipitation syntheses have been widely employed for morphology controlled Cu_2O even though low chemical stability in acidic conditions has been recognized as a drawback of Cu_2O in synthetic and application processes.[18–21] On the other hand, few studies have been reported on their etching behaviour, although their chemical stability is related to the surface etching reaction. Recently, Zhiyu and co-workers reported the conversion of cuprous oxide nanocrystals to SnO_2 nanoboxes *via* a coordinating etching process.[4] Unfortunately, there have been no reports on the effect of surfactants on the facet selective oxidative etching (FSOE) reaction with transition metal ions (Fe^{n+} or Co^{n+}) to our best knowledge.

Korea Center for Artificial Photosynthesis, Department of Chemistry, Sogang University, Seoul, 121-742, Republic of Korea. E-mail: yskang@sogang.ac.kr; Fax: +82 2 701 0967; Tel: +82 2 701 6379

† Electronic supplementary information (ESI) available: TEM and SEM images of PVP–Cu_2O and nPVP–Cu_2O, FTIR result of PVP and PVP–Cu_2O *etc.* See DOI: 10.1039/c3nr03626j

Herein, we propose hollow metal oxide nanocrystals by etching cuprous oxide with metal(II) ions based on the chemical instability of Cu_2O in acidic media, which is able to progress at room temperature (RT). Especially, we report the coordination-dependent etching behaviour of both surfactant stabilized and non-surfactant assisted octahedral cuprous oxide nanocrystals using Fe^{2+} or Co^{2+} ions, which form hematite and Co_3O_4 hollow structured octahedral nanoboxes through further annealing of the as-formed amorphous state of metal oxide structures. Compared with the high temperature annealing process for achieving hollow structured metal oxides, this approach does not need high temperature treatment. Also, the FSOE behaviour that builds up a hierarchical hollow structure inside of the particles with non-surfactant assisted Cu_2O, was demonstrated. Moreover, using these etched hollow nanocrystals, a metal oxide monolayer film was fabricated with a secondary growth approach and was studied for its photocatalytic properties. Simultaneously, we demonstrate our motivation for Fe_2O_3 and Co_3O_4 hollow structures for application as photoanodes.

Experimental section

Fabrication of truncated octahedral cuprous oxide nanocrystals stabilized with and without surfactant

Surfactant-stabilized cuprous oxide nanocrystals were synthesized with minor modification to Zhang's method.[15] In a typical synthesis, 1.677 g of PVP (polyvinylpyrrolidone, M_w = 29 000) was dissolved in 50 mL of 0.01 M $CuCl_2$ solution. The solution was stirred for 1 h at RT to ensure homogeneity. 5 mL of 2 M NaOH solution was then injected dropwise with vigorous stirring. After 30 min, 5 mL of 0.6 M ascorbic acid was added to the above solution to reduce the copper hydroxide complex. The blue copper hydroxide solution then transformed to a reddish brown color in 5 min. The reaction was finished within 3 h. The resulting particles were centrifuged in 5000 rpm for 5 min and washed with distilled water (D.W.) and ethanol several times. Decanted powder was dried in a vacuum oven at 80 °C. For comparison of the etching effect between the presence and absence of surfactant, truncated octahedral cuprous oxide was synthesized by altering the reaction temperature and reducing agent without surfactant.[18] 10 mL of 0.1 M copper(II) acetate and 10 mL of 3 M NaOH were mixed to form copper hydroxide and stirred for 10 min at RT. The mixed solution was then slowly heated up to 70 °C in an oil bath. At the same temperature, 5 mL of 2 M D-glucose solution was added dropwise into black precipitated solution and stirred for another 1 h. Red precipitate was obtained by centrifugation and washed with D.W. and ethanol several times. The powder was dried in a vacuum oven at 80 °C for 1 h and used to carry out the etching reaction of cuprous oxide nanocrystals with transition metal ion solutions.

Etching reaction of Cu_2O nanocrystals for the synthesis of hollow metal oxide structures

Each of the previously synthesized cuprous oxide powders (0.02 g) was re-dispersed in 10 mL of absolute ethanol. 0.3 mL of 1.71 M NaCl in D.W. solution was added to 10 mL of 2 mM MCl_2 (M = Fe, Co, Ni) and a $TiCl_4$ ethanol solution was slowly added into the above solution. The overall reaction was completed in 10 min and the etching process was confirmed by the color change of the transition metal chloride solution. The final product of the precipitate was centrifuged, washed, and dried as stated previously. Completely etched powder was annealed at 500 °C for 5 h with an increasing temperature rate of 10 °C min^{-1}.

Characterization

The morphology and size of as-prepared cuprous oxide and metal oxide particle were characterized by scanning electron microscopy (SEM, the Cold Field Emission Scanning Electron Microscope Hitachi S-4300). X-ray diffraction (XRD, Cu Kα radiation (λ = 1.54056 Å) using a Rigaku X-ray diffractometer operating at 40 kV and 150 mA at a scanning rate of 0.02° per step in the 2θ range of $20° \leq 2\theta \leq 80°$) was used to characterize the crystal structure of Cu_2O nanocrystals. Hollow structured Cu_2O and its elemental analysis were characterized by transmission electron microscopy (TEM, JEOL, JEM-2010, and JEOL JEM 2100F, operated at 200 kV).

Photocurrent measurements

The photoelectrochemical measurements of Fe_2O_3 or Co_3O_4 film electrodes (dimension = 0.5 cm^2) as photoanodes were obtained using potentiostat (Physio Lab PL-9) with a three-electrode cell (1 M KOH (pH 13.6) as electrolyte, Pt wire as a counter electrode and Ag/AgCl as a reference electrode in saturated KCl). A 300 W Xenon lamp (Asahi Spectra HAL-320, ozone free) was illuminating the photoanode with a HAL AM 1.5G filter at a measured distance for 1 sun intensity (100 mW cm^{-2}, spectrally corrected).

Results and discussion

Etching behavior of truncated octahedral cuprous oxide nanocrystals stabilized with PVP

For investigation of a transition metal ion's etching ability, PVP (polyvinylpyrrolidone) stabilized Cu_2O sub-micron crystals (PVP–Cu_2O) were synthesized *via* a precipitation method. Fig. 1(a) shows an SEM image of truncated octahedral cuprous oxide nanocrystals, with 600 nm long edges of the octahedra, and their degree of dispersion with PVP. In the precipitation method, ascorbic acid was used to initiate the reduction of the copper hydroxide complex, $[Cu(OH)_4]^{2-}$, forming a Cu_2O crystal structure. The amount of PVP was used to control the morphology of Cu_2O from cubic to octahedral. It means that total area of {111} facets increased simultaneously as the amount of PVP increased (ESI, Fig. S1†). In comparison, two kinds of facet, such as {111} and {100}, exist in the Cu_2O particles synthesized by the precipitation method. Single Cu_2O particles were controlled by a {111} facet because {111}-dominant octahedral Cu_2O has a higher surface reactivity than that of the {100}-dominant cubic morphology.[22] The {100} facet is composed of six surface facets and the {111} facet is composed of eight surface facets of truncated octahedral Cu_2O marked on the schematic illustration in Fig. 1 and 2. Oxygen atoms in the carbonyl group (C═O) of PVP

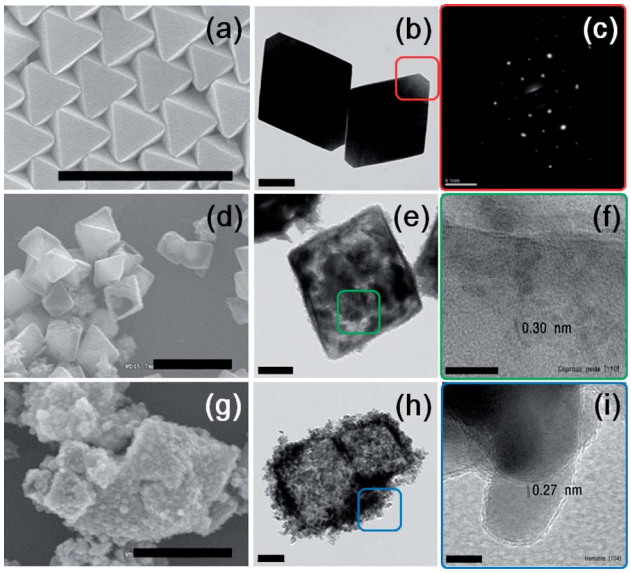

Fig. 1 SEM and HR-TEM images of PVP stabilized cuprous oxide (a–c), metal ion etched structures after 3 h (d–f) and for 24 h (g–i). Scale bar, 2 μm in SEM images (a, d and g), 200 nm in TEM images (b, e and h), 5 nm in HRTEM images (f) and (i).

coordinate with coordination unsaturated copper (Cu_{CUS}) at the surface of the {111} facets to suppress oxidization by binding the oxygen in air, as shown in Fig. S2.†[23,24]

Interestingly, the self-assembled ordered arrays of PVP–Cu_2O were observed due to its PVP functionalized surface. Self-assembly of PVP–Cu_2O crystals occurred *via* slow evaporation of solvent in the Cu_2O particle solution which were dispersed in a mixture of ethanol and D.W. This phenomenon arose from the van der Waals interaction among PVP's carbonyl groups at the surface. The self-assembling behavior of hexadecylamine (HDA)-stabilized Cu_2O has been reported from the view of the functional groups on the surface.[25] The TEM image and its selected area electron diffraction (SAED) pattern verifies the single crystalline structure of Cu_2O in Fig. 1(c).

The overall etching reaction equation and process of Cu_2O are demonstrated in Fig. 2. A cationic exchange reaction occurs during etching of Cu_2O resulting in iron oxide hydrate and

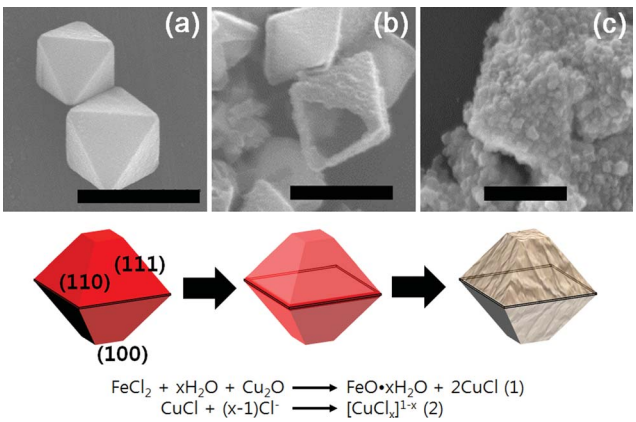

Fig. 2 Schematic presentation of the metal ion based conversion process from PVP stabilized cuprous oxide to iron oxide with a hollow structure. Scale bar, 1 μm.

copper(I) chloride. Due to rapid dissolution of Cu_2O in acidic conditions, the etching reaction in acidic media was performed in an organic medium to control the rate of reaction. In an excess organic medium, such as ethanol, the low release of ionic precursors such as Fe^{2+} and Cl^- ions are the driving force for the interfacial reaction to form copper based complexes such as CuCl or $[CuCl_x]^{1-x}$. The ionic state of transition metal ions as a driving force for the oxidative etching reaction of copper ions is due to the higher Lewis acidity. In the presence of iron(II) on the surface of Cu_2O, oxidation of iron(II) and reduction of copper(I) occur at the same time through transportation of oxygen from copper to iron(II). During the reaction (less than 12 h) hollow cuprous oxide structures were formed with an amorphous iron oxide state. Exterior shrinkage was observed in the SEM images and one of the {111} facets was missing in some particles, as shown in Fig. 1 and 2. TEM and HR-TEM of Cu_2O reveal that the PVP stabilized exterior of octahedral Cu_2O retains its octahedral shape in Fig. 1(e) and (f). The lattice distance was 0.30 nm, indicating a (110) plane of cuprous oxide. Even after the etching reaction, the crystallinity of the initial state was unchanged. With an increased reaction time of 24 h, the hollow Cu_2O template is completely converted to amorphous iron oxide or cobalt oxide, shown in Fig. 1(g), (h) and (i). After complete conversion of Cu_2O to the amorphous state by the annealing process, α-Fe_2O_3 particles smaller than 500 nm in diameter were formed on the exterior of the hollow template and its lattice distance was 0.27 nm as a (104) plane of hematite in Fig. 1(e) and (f). During the etching reaction, the thermal energy is not provided for crystal structure formation, thus the crystalline patterns of α-Fe_2O_3 or Co_3O_4 crystal structures were detected after annealing at 500 °C for 5 h (Fig. 8). Copper chloride complexes, CuCl and $[CuCl_x]^{1-x}$, as reaction intermediates are soluble in hydrophilic media, thus repeated washing of the reaction intermediates does not provide copper oxide crystal peaks in the XRD results. A previous study from Zou's group reported on the etching of PVP stabilized Cu_2O *via* aging for longer times such as 16 h.[12] However, in the present study, the acidic etching of PVP stabilized Cu_2O with transition metal ions was completed in less than 1 h. Furthermore, it is feasible to control the rate of reaction by adjusting the concentration of metal precursors in ethanol through releasing a vast amount of an ionic component in organic media. The possible formation of the Cu_2O hollow template is simply caused by the role of the surfactant, PVP, which forms surface facets of octahedral Cu_2O. As indirect evidence, the presence of PVP on the Cu_2O surface suppresses the binding of oxygen with Cu_{CUS}. It results in the higher stability of PVP–Cu_2O for thermal oxidation compared to Cu_2O without surfactant. This cannot confirm the etching reaction at the surface facets of {100} and {111} of Cu_2O. Fig. 3 shows TEM and EDS elemental mapping images of hollow α-Fe_2O_3 and Co_3O_4 structures.

Etching behavior of truncated octahedral cuprous oxide crystals without surfactant

To eliminate the influence of the surfactant on the etching reaction, thermal and chemical treatments were applied.

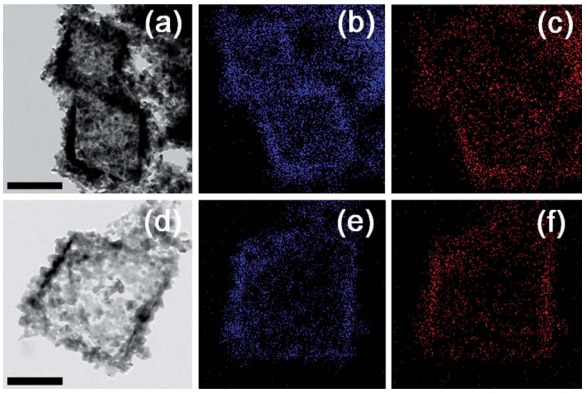

Fig. 3 TEM and elemental mapping images of α-Fe_2O_3 ((a and b) Fe elemental mapping and (c) O elemental mapping) and Co_3O_4 ((d and e) Co elemental mapping and (f) O elemental mapping) hollow structures, fabricated by the metal ion etching reaction. Scale bar, 400 nm.

Unfortunately, it was impossible to completely eliminate these kinds of polymer surfactants *via* thermal or chemical treatment without changing the morphology and phase of Cu_2O. During the thermal process, the oxidation of cuprous oxide occurred in addition to the carbonization of the polymer. With inert gas conditions, the phase was not changed. However, the octahedral shape changed at 500 °C. Hydrazine was also used to eliminate the polymer surfactant.

Non-surfactant assisted Cu_2O (nPVP–Cu_2O) was synthesized to investigate the etching behavior in each facet of a single particle. Thus, nPVP–Cu_2O was fabricated *via* a different method. The amount of glucose, as a reducing agent, and the reaction temperature are the main factors to control morphology by this approach. The SEM images of the synthesized truncated octahedral morphology of Cu_2O with 500 nm edge length are shown in Fig. 4 and S3†. The etching reaction of nPVP–Cu_2O was carried out in the aforementioned way. As reaction time increased, an uncommon transformation behavior was observed with nPVP–Cu_2O compared to PVP–Cu_2O. As shown in Fig. 4(a)–(c), truncated octahedral Cu_2O particles mainly consist of 8 {111} facets with the largest surface area, and the truncated area consists of 6 {100} facets. As the SEM images show, only {100} and {110} facets are etched *via* the Fe^{2+} ion exchange reaction. {111} facets were not etched even without the presence of surfactant, PVP. This phenomenon infers that Fe^{2+} ions have undergone selective oxidative facet etching, as shown in Fig. 4(a)–(c).

For further investigation, several kinds of transition metal ion precursors such as $CoCl_2$, $NiCl_2$ and $TiCl_4$ were examined in the same way. Also, to avoid the anionic precursor effect, all metal precursors with the same chloride anion were used. In the case of $TiCl_4$, an uncontrollable reaction occurred due to the high oxidation state (4+) of titanium. Thus, it was impossible to control the morphology of the resulting template. However, metal precursors with a low oxidation state (2+) such as Co^{2+} allow control of the reaction rate. This can be identified with TEM images in Fig. 5(a)–(d). Co(II) has a different etching behavior compared with Fe^{2+} which has facet selectivity. Therefore, as is shown in the TEM image, hierarchical structures of amorphous cobalt oxide substances cover the surface of nPVP–Cu_2O. The crystal lattice was identified in the inset of the aggregated assembly. Similar results appeared with Ni^{2+} etching, shown in Fig. 5(e) and (f). Unlike Fe^{2+}, two metal ions (Co^{2+} and Ni^{2+}) reacted at the surface of the Cu_2O particle without selective oxidative facet etching because of the higher oxygen affinity by higher Lewis acidities. Compared with the PVP–Cu_2O results, etching of nPVP–Cu_2O with Fe^{2+} produces selectively etched hollow particles on the facet surface with stabilized surfactant. From the above results, it is possible to conclude that the higher facet reactivity of {100} allows the etching reaction in the presence of PVP, but it does not allow the etching reaction of the {110} facet in the presence of PVP. On the other hand, it allows the etching reaction of both facets of Cu_2O in the absence of PVP. The etching reaction of the {111} facet Cu_2O does not occur in both reactions with or without PVP. The function of PVP is to suppress the etching reactivity selectively on the {110} facet. This facet selective etching reaction is also found in Fig. 1(d) as one selectively facet-opened particle as mentioned above. The loss of one facet in the hollow structure led to a possible mass transfer through the interface of the hollow structure to enlarge the reactive surface area. Fig. 6 shows a schematic presentation of the PVP–Cu_2O (a) and nPVP–Cu_2O (b) etching reaction behavior by metal(II) ions.

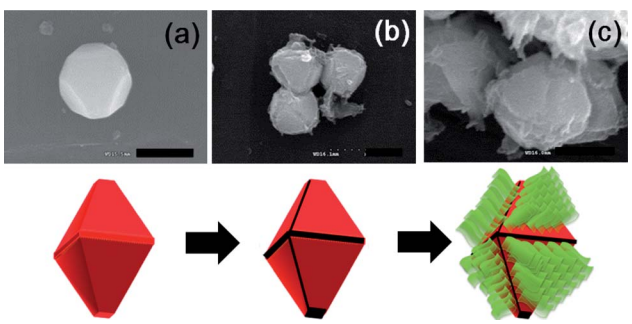

Fig. 4 Schematic presentation of a metal ion conversion process from a non-surfactant stabilized cuprous oxide to a hierarchical structure of a metal oxide–cuprous oxide composite. SEM images of cuprous oxide (a), a metal ion etched structure after 0.5 h (b) and after 1 h (c). Scale bar, 500 nm.

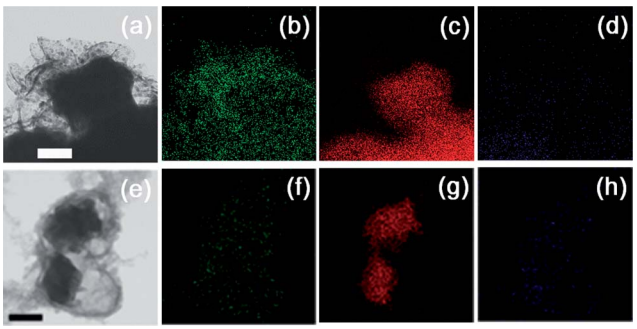

Fig. 5 TEM and elemental mapping images of the etched nPVP–Cu_2O by Co^{2+} ((a and b) Co elemental mapping, (c) Cu elemental mapping and (d) O elemental mapping) and Ni^{2+} ((e and f) Ni elemental mapping, (g) Cu elemental mapping and (h) O elemental mapping) for 2 h. Scale bar, 200 nm.

Crystallographic and photocatalytic application

The crystallographic structure of PVP–Cu_2O, Cu_2O, Fe^{2+} etched Cu_2O, and Co^{2+} etched Cu_2O were examined by XRD (Fig. S4† and 8, JCPDS #78-2076). The XRD patterns of PVP–Cu_2O and Cu_2O show that it has a highly crystalline structure. The relative intensity difference reveals that the octahedral morphology has a higher surface area of the (111) facet. After the controlled etching reaction of Cu_2O with Fe^{2+} and Co^{2+} ions, no other metal oxide crystal structure was found because the RT reaction does not allow the crystal structure change. SOFE could be explained in several ways. Galvanic potential difference between the copper ion of Cu_2O and other metal ion is a driving force for the etching reaction. The repulsion between the cations of the etching reactant and etchant reactant, caused by unsaturated coordination of copper (Cu_{CUS}), can be another important factor to explain SOFE. Huang *et al.* demonstrated structural modeling of a Cu_2O crystal.[23,24] The {100} facet is terminated with oxygen atoms which bind to copper in a fully coordinated state, thus there are two types of atoms fully coordinated with each other. On the other hand, the {111} facet is terminated with both copper and oxygen atoms. Of note, copper is not fully coordinated with oxygen on the surface. Due to its cationic properties, unsaturated copper prefers to be coordinated with other anionic substances. This is the reason that the cubic shape of Cu_2O has higher stability than the octahedral shape. Inversely, the (111) plane in the octahedra has higher catalytic activity due to Cu_{CUS} binding with reactants.

Further application of the etching reaction possibly results in the fabrication of a hollow structured monolayer of α-Fe_2O_3 and Co_3O_4 as shown in Fig. 7 and 8. Manual assembly and secondary growth[26] (2^{nd} growth) can give controlled thickness single crystal films of zeolite or hematite.[27] However, films of metal oxide structures can provide only 1-D surfaces for the surface reaction *via* photocatalytic reaction. The low thermal stability of cuprous oxide makes it difficult to eliminate polyethyleneimine (PEI), which is a surface directing agent for manual assembly, through the calcination process. Compared with secondary growth, the etching process possibly results in filling the gap between the oriented particles. TEM images in Fig. 1(h) also support that α-Fe_2O_3 crystals were formed at the external surface of the hollow template with 100–200 nm thickness.

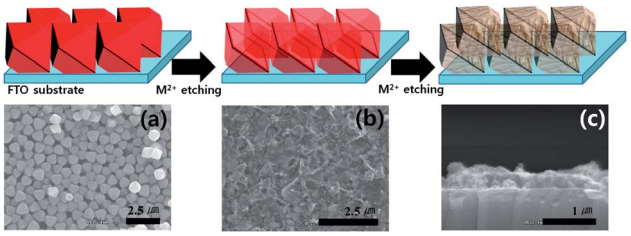

Fig. 7 Schematic presentation of fabrication process for mono layered metal oxide film (upper row). SEM images of (111)-axis opened Cu_2O monolayer (a) and hollow structured α-Fe_2O_3 film (top view (b), cross-sectional view (c)).

For photocatalytic application, absorption behavior at the visible range was measured in reflectance mode to define the band gap of the resulting metal oxides. As shown in Fig. 8(b) and S5,† optical absorptions of α-Fe_2O_3, Co_3O_4 and Cu_2O occurred in the visible range. The band gaps of semiconductor material were determined by plotting the Kubelka–Munk equation[28] with UV-vis absorption spectra. Determinations of band gap energies resulted in 1.9 eV of Cu_2O, 2.07 eV of α-Fe_2O_3 and 1.80 eV of Co_3O_4. The determined values fall in the range of the previously reported band gap values. Conversion of a Cu_2O monolayer with Fe or Co cations resulted in gap filling between particles. The formation of α-Fe_2O_3 or Co_3O_4 nanocrystals occurred in the exterior of the octahedral template of Cu_2O. From Fig. 7(a), the one-axis oriented monolayer of Cu_2O has an empty space range from 100 to 300 nm in length. The thickness of α-Fe_2O_3 which composes the exterior of octahedral template is longer than 100 nm. Filled α-Fe_2O_3 film is shown in Fig. 7(b) and (c), with top and cross-section views. Due to the photocatalytic ability of α-Fe_2O_3 and Co_3O_4, linear sweep voltammetry experiments were carried out with irradiation of visible light.

All photoelectrochemical measurement were employed under a three electrode system using Ag/AgCl as the reference electrode, 1 M KOH solution as the electrolyte and platinum wire as the counter electrode. Photocurrent density was recorded as a function of applied voltage under visible light. Fig. 9 shows that photocurrent densities are higher in reduction (anodic) potential. The *I–V* curve of each hollow structured

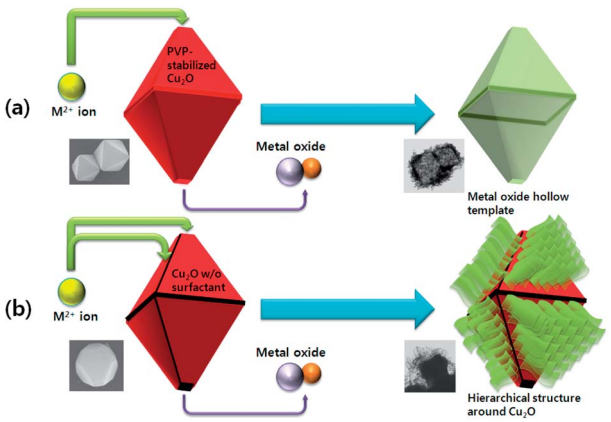

Fig. 6 Schematic presentation of the PVP–Cu_2O (a) and nPVP–Cu_2O (b) etching reaction behavior by metal(II) ions.

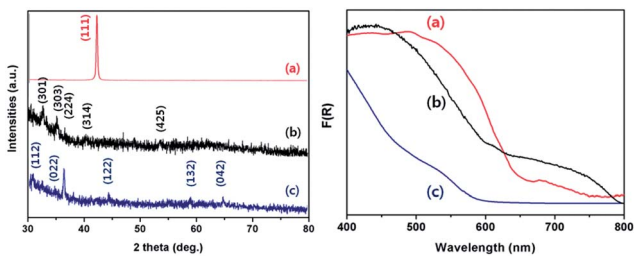

Fig. 8 XRD and UV-vis measurement of Cu_2O (a), α-Fe_2O_3 (b) and Co_3O_4 (c) films in reflectance mode.

photoanode was measured under dark and light illumination on the front-side. The photoresponse under dark of hollow structured Fe_2O_3 photoanode is almost negligible up to about 0.4 V *vs.* Ag/AgCl in Fig. 9(a). The photocurrent rises steeply at 0.1 V with illumination and become 5 μA at −0.4 V in Fig. 9(b). These results are the same for both α-Fe_2O_3 and Co_3O_4 films. Usually, α-Fe_2O_3 is an n-type material which has a flow of the excited electrons to the electrode (FTO). However, the results indicate that excited electrons are flowing from the α-Fe_2O_3 to electrolyte. This is mainly from the copper doping effect[29] on the surface of α-Fe_2O_3. During the fabrication of α-Fe_2O_3 film, the etching reaction was maintained without stirring. Fig. 9(c) and (d) show the photoresponse of a hollow structured Co_3O_4 photoanode with 1 μA at −0.2 V. Most copper complexes are soluble however there is some copper left in the hollow template. The amount of copper in α-Fe_2O_3 is not effective for the crystal structures. From the EDS data (Fig. S6†), we can conclude that to affect photocurrent behavior the copper has to remain at less than 10 wt%.

Conclusions

In summary, octahedral hollow structures of α-Fe_2O_3 and Co_3O_4 nanocrystals were fabricated from the etching reaction of PVP stabilized Cu_2O with Fe^{2+} and Co^{2+} ions. Because of their higher Lewis acidity, the cationic exchange reaction happens between the divalent metal ion and Cu^{+}. Facet selective etching of cuprous oxide has been observed during the ionic exchange reaction of Cu^{+} and O^{2-} ions in PVP–Cu_2O complexes with divalent transition metal ions at the (110) facet surface. In half of the reaction time, Cu_2O crystals remain at the external surface of the hollow template. After complete conversion of Cu^{2+} with other metals such as Fe^{2+} or Co^{2+}, the amorphous metal oxide was annealed for crystallization. With the synthetic mechanism of hollow structured α-Fe_2O_3 and Co_3O_4 nanocrystals, metal oxide monolayer films were fabricated on the FTO substrate for a semiconductor photoelectrode with a secondary growth approach. Clusters of iron oxide and cobalt oxide nanocrystals in the hollow template have profitable band gap energy values for semiconductors. It is noted that this approach would be promising for water splitting and catalytic photoelectrodes.

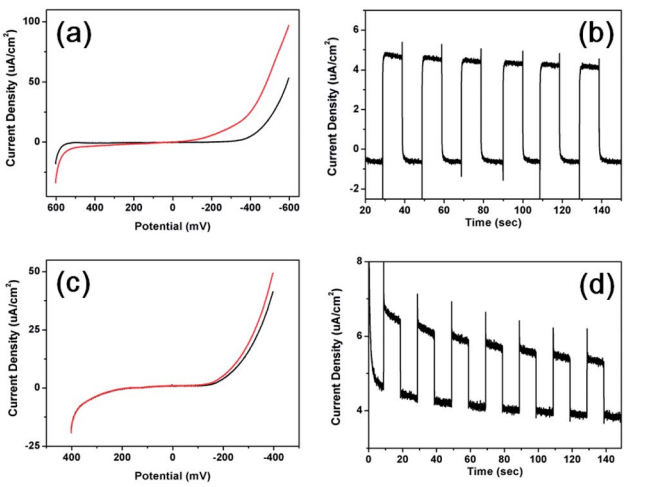

Fig. 9 Photocurrent current–potential characteristics by linear sweeping voltammetry of α-Fe_2O_3 (a) and Co_3O_4 films (c) under visible light. Visible light photoresponse of α-Fe_2O_3 (b) and Co_3O_4 films (d).

Acknowledgements

This work was supported by the Korea Center for Artificial Photosynthesis (KCAP) located in Sogang University funded by the Ministry of Education, Science, and Technology (MEST) through the National Research Foundation of Korea (no. 2012M1A2A2671783).

Notes and references

1 H. G. Yang, C. H. Sun, S. Z. Qiao, J. Zou, G. Liu, S. C. Smith, H. M. Cheng and G. Q. Lu, *Nature*, 2008, **453**, 638; T.-D. Nguyen and T.-O. Do, Size- and Shape-Controlled Synthesis of Monodisperse Metal Oxide and Mixed Oxide Nanocrystals, *Nanocrystal*, ed. Y. Masuda, 2011.
2 X. W. Lou, L. A. Archer and Z. Yang, *Adv. Mater.*, 2008, **20**, 3987; F. Caruso, R. A. Caruso and H. Mohwald, *Science*, 1998, **282**, 1111; P. V. Kamat, K. Tvrdy, D. R. Baker and J. G. Radich, *Chem. Rev.*, 2010, **110**, 6664; C. N. R. Rao, A. Müller and A. K. Cheetham, *Nanomaterials – An Introduction*, Wiley-VCH Verlag GmbH & Co. KGaA, 2005; S. Abbet and U. Heiz, *Nanocatalysis*, Wiley-VCH Verlag GmbH & Co. KGaA, 2005.
3 X. Lai, J. Li, B. A. Korgel, Z. Dong, Z. Li, F. Su, J. Du and D. Wang, *Angew. Chem.*, 2011, **12**, 279.
4 Z. Wang, D. Luan, F. Y. C. Boey and X. W. Lou, *J. Am. Chem. Soc.*, 2011, **133**, 4738.
5 S. Liu, J. Yu and M. Jaroniec, *J. Am. Chem. Soc.*, 2010, **132**, 11914.
6 J. Qian, P. Liu, Y. Xiao, Y. Jiang, Y. Cao, X. Ai and H. Yang, *Adv. Mater.*, 2009, **21**, 3663.
7 C. R. Martin and P. Kohli, *Nat. Rev. Drug Discovery*, 2003, **2**, 29; Z. P. Xu, Q. H. Zeng, G. Q. Lu and A. B. Yu, *Chem. Eng. Sci.*, 2006, **61**, 1027; V. Sokolova and M. Epple, *Angew. Chem., Int. Ed.*, 2008, **47**, 1382.
8 S. W. Kim, M. Kim, W. Y. Lee and T. Hyeon, *J. Am. Chem. Soc.*, 2002, **124**, 7642; S. Ikeda, S. Ishino, T. Harada, N. Okamoto, T. Sakata, H. Mori, S. Kuwabata, T. Torimoto and M. Matsumura, *Angew. Chem., Int. Ed.*, 2006, **45**, 7063; H. P. Liang, H. M. Zhang, J. S. Hu, Y. G. Guo, L. J. Wan and C. L. Bai, *Angew. Chem., Int. Ed.*, 2004, **43**, 1540.
9 Y. Yin, R. M. Rioux, C. K. Erdonmez, S. Hughes, G. A. Somorjai and A. P. Alivisatos, *Science*, 2004, **304**, 711.
10 H. Cao, X. Qian, C. Wang, X. Ma, J. Yin and Z. Zhu, *J. Am. Chem. Soc.*, 2005, **127**, 16024.
11 K. An, S. G. Kwon, M. Park, H. B. Na, S. I. Baik, J. H. Yu, D. Kim, J. S. Son, Y. W. Kim and I. C. Song, *Nano Lett.*, 2008, **8**, 4252.
12 Y. Sui, W. Fu, Y. Zeng, H. Yang, Y. Zhang, H. Chen, Y. Li, M. Li and G. Zou, *Angew. Chem., Int. Ed.*, 2010, **49**, 4282.

13 H. Zhang, M. Jin, H. Liu, J. Wang, M. J. Kim, D. Yang, Z. Xie, J. Liu and Y. Xia, *ACS Nano*, 2011, **5**, 8212.
14 F. Hong, S. Sun, H. You, S. Yang, J. Fang, S. Guo, Z. Yang, B. Ding and X. Song, *Cryst. Growth Des.*, 2011, **11**, 3694.
15 D. F. Zhang, H. Zhang, L. Guo, K. Zheng, X. D. Han and Z. Zhang, *J. Mater. Chem.*, 2009, **19**, 5220.
16 C. H. Kuo and M. H. Huang, *J. Am. Chem. Soc.*, 2008, **130**, 12815.
17 M. Cao, C. Hu, Y. Wang, Y. Guo, C. Guo and E. Wang, *Chem. Commun.*, 2003, 1884.
18 S. Sun, F. Zhou, L. Wang, X. Song and Z. Yang, *Cryst. Growth Des.*, 2009, **2**, 541.
19 X. Lan, J. Zhang, H. Gao and T. Wang, *CrystEngComm*, 2011, **13**, 633.
20 C. H. Kuo, C. H. Chen and M. H. Huang, *Adv. Funct. Mater.*, 2007, **17**, 3773.
21 C. M. McShane, W. P. Siripala and K. S. Choi, *J. Phys. Chem. Lett.*, 2010, **1**, 2666.
22 H. Xu, W. Wang and W. Zhu, *J. Phys. Chem. B*, 2006, **110**, 13829.
23 H. Bao, W. Zhang, D. Shang, Q. Hua, Y. Ma, Z. Jiang, J. Yang and W. Huang, *J. Phys. Chem. C*, 2010, **114**, 6676.
24 Q. Hua, D. Shang, W. Zhang, K. Chen, S. Chang, Y. Ma, Z. Jiang, J. Yang and W. Huang, *Langmuir*, 2011, **27**, 665.
25 K. X. Yao, X. M. Yin, T. H. Wang and H. C. Zeng, *J. Am. Chem. Soc.*, 2010, **132**, 6131.
26 J. Lee, J. Kim, Y. Lee, N. Jeong and K. Yoon, *Angew. Chem.*, 2007, **119**, 3147.
27 H. G. Cha, J. Song, H. S. Kim, W. Shin, K. B. Yoon and Y. S. Kang, *Chem. Commun.*, 2011, **47**, 2441.
28 J. H. Nobbs, *Rev. Prog. Color. Relat. Top.*, 1985, **1**, 66.
29 W. B. Ingler Jr and S. U. M. Khan, *Int. J. Hydrogen Energy*, 2005, **30**, 821.